Wnt11 controls cell contact persistence by local accumulation of Frizzled 7 at the plasma membrane

Sabine Witzel,[1] Vitaly Zimyanin,[1] Filipa Carreira-Barbosa,[2] Masazumi Tada,[2] and Carl-Philipp Heisenberg[1]

[1]Max-Planck-Institute of Molecular Cell Biology and Genetics, 01307 Dresden, Germany
[2]Department of Anatomy and Developmental Biology, University College London, London WC1E 6BT, England, UK

Wnt11 is a key signal, determining cell polarization and migration during vertebrate gastrulation. It is known that Wnt11 functionally interacts with several signaling components, the homologues of which control planar cell polarity in *Drosophila melanogaster*. Although in *D. melanogaster* these components are thought to polarize cells by asymmetrically localizing at the plasma membrane, it is not yet clear whether their subcellular localization plays a similarly important role in vertebrates. We show that in zebrafish embryonic cells, Wnt11 locally functions at the plasma membrane by accumulating its receptor, Frizzled 7, on adjacent sites of cell contacts. Wnt11-induced Frizzled 7 accumulations recruit the intracellular Wnt signaling mediator Dishevelled, as well as Wnt11 itself, and locally increase cell contact persistence. This increase in cell contact persistence is mediated by the local interaction of Wnt11, Frizzled 7, and the atypical cadherin Flamingo at the plasma membrane, and it does not require the activity of further downstream effectors of Wnt11 signaling, such as RhoA and Rok2. We propose that Wnt11, by interacting with Frizzled 7 and Flamingo, modulates local cell contact persistence to coordinate cell movements during gastrulation.

Introduction

Wnts play key roles in cell polarization and migration during vertebrate gastrulation, by signaling through a noncanonical pathway similar to the Frizzled (Fz) signaling pathway that determines epithelial planar cell polarity (PCP) in *Drosophila melanogaster* (Strutt, 2003). An essential step during Fz/PCP-driven cell polarization in *D. melanogaster* is the localization of PCP components, including the receptor Fz, to specific sites of the cell cortex (Adler, 2002). Such subcellular localization of vertebrate PCP components during Wnt-dependent cell polarization and migration has not yet been reported, and the cellular mechanisms by which Wnt/PCP signaling acts remain poorly understood.

Increasing evidence suggests that noncanonical Wnts control cell migration by regulating cell adhesion. Ectopic Wnt5 expression decreases cell adhesion in cultures of dissociated dorsal mesoderm from *Xenopus laevis* gastrulas (Torres et al., 1996). Additionally, "knocking down" the presumed Wnt11 receptor Frizzled 7 (Fz7) in *X. laevis* embryos causes defects in germ layer separation at the onset of gastrulation (Winklbauer et al., 2001). Fz7 appears to function in this process by interacting with paraxial protocadherin C to control differential adhesiveness between the germ layers (Medina et al., 2004; Unterseher et al., 2004). Wnt11 itself has recently been shown to modulate the de-adhesion forces needed to separate zebrafish mesendodermal progenitors from substrates decorated with fibronectin and E-cadherin (Puech et al., 2005; Ulrich et al., 2005).

Our previous work shows that during zebrafish gastrulation Wnt11 is required for the polarization and coherent migration of prechordal plate progenitors (Ulrich et al., 2003, 2005). The prechordal plate derives from mesodermal and endodermal cells (mesendoderm) that internalize at the dorsalmost germ ring margin, where the embryonic organizer (shield) forms, and then migrate as a coherent group of mesenchymal cells along the overlying ectodermal layer toward the animal pole (Warga and Kimmel, 1990; Montero et al., 2005). We recently provided evidence that Wnt11 controls cell cohesion of prechordal plate progenitors by modulating the subcellular localization of E-cadherin in these cells (Ulrich et al., 2005). Although such a mechanism could serve to globally regulate cell cohesion, it remains to be established whether Wnt11 possesses a more direct function in the local control of cell contact behavior.

In this study, we show that Wnt11 controls cell contact persistence of gastrulating zebrafish cells at a local level by

Correspondence to Carl-Philipp Heisenberg: Heisenberg@mpi-cbg.de; or Masazumi Tada: M.Tada@ucl.ac.uk

Abbreviations used in this paper: hpf, h after fertilization; MO, morpholino; PCP, planar cell polarity.

The online version of this article contains supplemental material.

The Journal of Cell Biology, Vol. 175, No. 5, December 4, 2006 791–802
http://www.jcb.org/cgi/doi/10.1083/jcb.200606017

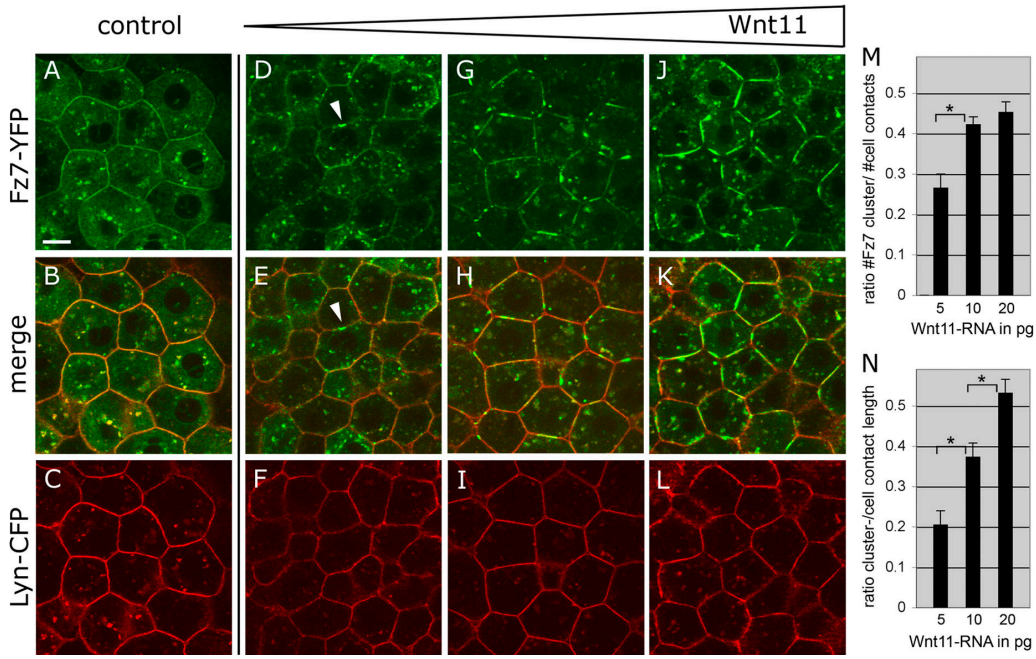

Figure 1. **Wnt11 induces local accumulation of Fz7 at the plasma membrane.** (A–L) Coexpression of *fz7-yfp* in green and membrane marker *lyn-cfp* in red (60 pg mRNA each) in the animal pole assay (pregastrula-stage embryos, 5 hpf) in the absence (A–C) and presence (D–L) of 5 (D–F), 10 (G–I), or 20 pg (J–L) of *wnt11* mRNA. Arrowheads mark Fz7 accumulation at the plasma membrane. (M) Ratio of Fz7-YFP accumulations at the plasma membrane/cell contact number (2D quantification; 70 cells total from seven embryos were used per condition). (N) Ratio of Fz7-YFP accumulation length/total cell contact length. Note that in control cells, Fz7-YFP accumulations were never seen (70 measurements total from six embryos were used per condition). Error bars represent the SEM. Asterisks demarcate statistically significant differences ($P < 0.05$). Bar, 10 μm.

determining the subcellular distribution of PCP components at the plasma membrane. We find that at cell contact points, Wnt11 triggers the accumulation of its receptor, Fz7, on apposing plasma membranes, along with the intracellular mediator Dsh and Wnt11 itself. These Wnt11-induced Fz7 accumulations increase cell contact persistence in a manner that is dependent on the activity of Flamingo (Fmi), which is an atypical cadherin, but independent of further downstream signaling by RhoA and Rok2. This work suggests that Wnt11 directly controls cell adhesion through local interactions with Fz7, Dsh, and Fmi at cell contacts.

Results

Wnt11 accumulates Fz7 and Dsh at cell contacts

To address the effects of Wnt11 signaling on cell behavior within the zebrafish embryo, we first fused fluorescent proteins (CFP and YFP) to the C terminus of Wnt11 pathway components, including Wnt11, its receptor Fz7, and its intracellular signaling mediator Dsh. *Fz7* and *Dsh* fusion constructs were designed as previously described (Yang-Snyder et al., 1996; Strutt, 2001). Wnt11-YFP activity was confirmed by its rescue of the *slb/wnt11* mutant phenotype (Table S1). Fusions of the zebrafish *fz7a* and *fz7b* homologues (Sumanas et al., 2000; El-Messaoudi and Renucci, 2001; Kudoh et al., 2001; Ungar and Calvey, 2002) behave identically in terms of subcellular localization; therefore, all data described in this study were obtained with tagged and untagged versions of *fz7a* (referred to as *fz7*).

To visualize Wnt11 pathway components in a simple cellular context, we injected our fusion constructs into one-cell–stage embryos and analyzed the resulting expression in animal pole blastoderm cells of pregastrula-stage embryos (30% epiboly; 5 h after fertilization [hpf]). Using this "animal pole assay," we avoided endogenous expression of *wnt11* and *fz7*, although maternal *fz7b* is present (Fig. S1, available at http://www.jcb.org/cgi/content/full/jcb.200606017/DC1).

To determine if Wnt11 regulates the subcellular distribution of Fz7, we analyzed Fz7-YFP localization in the presence of various amounts of Wnt11 under the animal pole assay conditions. Independent of Wnt11, Fz7-YFP localized uniformly at the plasma membrane and to cytoplasmic "puncta" (Fig. 1, A–C). In the presence of low amounts of *wnt11* (5–20 pg mRNA/embryo), however, Fz7-YFP accumulated into patches on the plasma membrane (Fig. 1, D–L). This effect appeared to be Fz7 specific, as the uniform distribution of membrane-bound YFP (Lyn-YFP), or another unrelated transmembrane receptor for FGF8 (FGF8R), did not change upon Wnt11 expression (Figs. S2 and S3, available at http://www.jcb.org/cgi/content/full/jcb.200606017/DC1). Moreover, Wnt11 induced Fz7-YFP accumulations in a concentration-dependent manner, with increased amounts of Wnt11 enhancing both the number and size of Fz7-YFP accumulations (Fig. 1, M and N). In contrast, high amounts of the *slb* mutant allele of *wnt11* (40 pg mRNA; $wnt11^{tx226}$), which encodes an inactive C-terminal truncated version of Wnt11 (Heisenberg et al., 2000), did not induce Fz7 accumulations (unpublished data). Additionally, high levels of Wnt3a, which is a canonical Wnt signal (50–100 pg

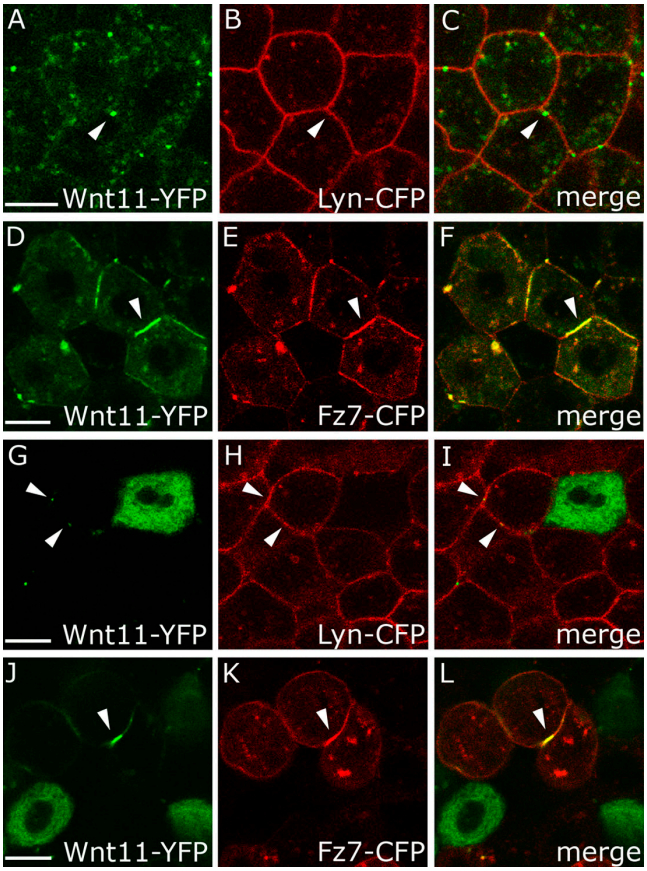

Figure 2. **Wnt11 locally accumulates with Fz7 at the plasma membrane.** (A–F) Coexpression of *wnt11-yfp* (50–100 pg mRNA) with *lyn-cfp* (60 pg mRNA; red; A–C) or *fz7-cfp* (110 pg mRNA; red; D–F) in the animal pole assay. Arrowheads mark Wnt11-YFP puncta at the plasma membrane (A–C) and Wnt11-YFP/Fz7-CFP–positive accumulations (D–F). (G–L) Wnt11-YFP–expressing (green) cells transplanted into host embryos expressing either Lyn-CFP (red; G–I) or Fz7-YFP (red; J–L). Arrowheads mark Wnt11-YFP puncta at host cell membrane (G–I) or Fz7-CFP/Wnt11-YFP–positive accumulations at host cell membrane. Bars: 10 μm.

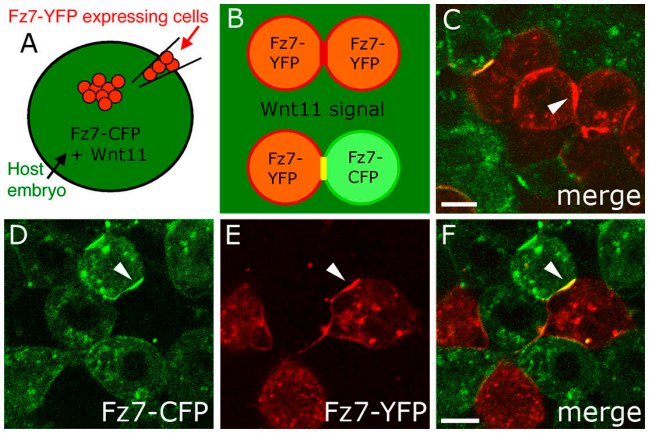

Figure 3. **Wnt11-induced Fz7 accumulations form on contacting plasma membranes.** (A–F) As diagramed (A and B), cells expressing *fz7-yfp* (60 pg mRNA; red) were transplanted into the animal pole of host embryos (4 hpf) coexpressing *fz7-cfp* (110 pg mRNA; green) and *wnt11* (20 pg mRNA) and imaged 1–3 h later. (C) Fz7-YFP accumulation (arrowhead) between transplanted donor cells induced by Wnt11 expressed in surrounding host cells. (D–F) Fz7 accumulation between donor and host cells form at both donor cell (red) and host cell membranes (arrowheads). Bars, 10 μm.

mRNA/embryo), did not result in recognizable changes of Fz7 distribution at the plasma membrane (unpublished data). These data indicate that Fz7 accumulation is both dependent on and specific to Wnt11 activity. Wnt11 is therefore able to influence Fz7 subcellular localization, a potential mechanism to locally regulate cell behavior.

Wnt11 has previously been shown to bind Fz7 (Djiane et al., 2000). To test the expectation that Wnt11 colocalizes with Fz7, we analyzed the subcellular localization of Wnt11-YFP along with Fz7-CFP in the animal pole assay (Fig. 2, A–F). To distinguish between cell-autonomous and nonautonomous Wnt11 activity, we also transplanted Wnt11-YFP–expressing cells into the animal pole of host embryos ubiquitously expressing either the plasma membrane marker Lyn-CFP (Fig. 2, G–I) or Fz7-CFP (Fig. 2, J–L). In the absence of Fz7 overexpression, Wnt11-YFP was predominantly found in cytoplasmic structures of Wnt11-producing cells, but could also be detected in small puncta at the plasma membrane of both Wnt11-producing (Fig. 2, A–C) and -receiving cells (Fig. 2, G–I). In contrast, in the presence of Fz7-CFP, Wnt11-YFP was found in both producing (Fig. 2, D–F) and receiving cells (Fig. 2, J–L) to be enriched at regions that colocalized with Fz7-CFP accumulations. These Wnt11-YFP accumulations were larger than the plasma membrane puncta found in the absence of exogenous Fz7 (Fig. 2, A–C and G–I). These observations suggest that Wnt11, by binding to Fz7, induces both cell-autonomously and nonautonomously local accumulations of Fz7 at the plasma membrane.

Wnt11-induced Fz7 accumulations predominantly localized to cell contacts, suggesting that Wnt11 locally functions at those sites. To investigate whether Fz7 accumulations form on both contacting plasma membranes or whether they are restricted to one cell, we transplanted Fz7-YFP–expressing cells into host embryos expressing both Wnt11 and Fz7-CFP (Fig. 3 A). Consistent with accumulation on both cells, Wnt11-induced Fz7 accumulations located between Fz7-CFP–positive host cells and Fz7-YFP–positive donor cells contained both Fz7-YFP and -CFP (Fig. 3, D–F). Importantly, Wnt11 induced Fz7 accumulations at host–host and donor–donor cell contact sites (Fig. 3, B and C; and not depicted), confirming our previous observation (Fig. 2) that Wnt11 acts both cell-autonomously and nonautonomously.

A crucial step in noncanonical Wnt signaling is the relocalization of Dsh from the cytoplasm to the plasma membrane, an event that also occurs in response to Fz7 overexpression (Rothbacher et al., 2000; Park et al., 2005). To test if Wnt11-induced Fz7 accumulations are sites of local Wnt11 activity, we looked for changes in Dsh localization. When coexpressed with Fz7, Dsh-YFP localized uniformly to the plasma membrane, as expected (Fig. 4 C). However, when Dsh-CFP was coexpressed with Fz7-YFP and Wnt11 (20 pg mRNA), it localized to the resulting Fz7-YFP accumulations (Fig. 4, D–F). This suggests that Wnt11-induced Fz7 accumulations are sites of Wnt11 activity.

In summary, Wnt11 induces the accumulation of its receptor Fz7 together with the intracellular-signaling mediator

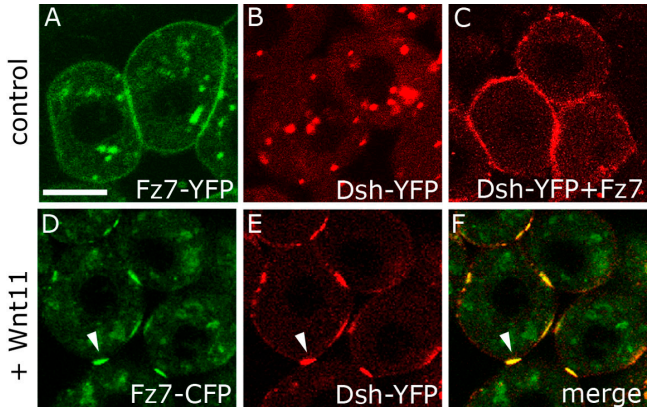

Figure 4. **Dsh is recruited to Wnt11-induced Fz7 accumulations.** (A–F) Animal pole assay in fixed embryos expressing either *fz7-yfp* (60 pg mRNA; A), *dsh-yfp* (75 pg mRNA; B), a combination of *dsh-yfp* and *fz7* (50 pg mRNA; C), or a combination of *dsh-yfp*, *fz7-cfp* (110 pg mRNA) and *wnt11* (20 pg mRNA; D–F). Arrowheads mark Fz7-CFP accumulations colocalizing with Dsh-YFP. Bar, 10 μm.

Dsh at the plasma membrane in regions of cell contact. Wnt11 may therefore act locally at cell contact sites to modulate cell behaviors.

Wnt11-induced Fz7 accumulations locally modulate cell contact dynamics

Wnt11 and Fz7 have previously been implicated in cell polarization and adhesion during *X. laevis* and zebrafish gastrulation (Winklbauer et al., 2001; Ulrich et al., 2003, 2005; Medina et al., 2004; Unterseher et al., 2004; Puech et al., 2005). To test whether Wnt11-induced Fz7 accumulations influence cell morphology or adhesion, we recorded 3D time-lapse videos of cells in the animal pole assay. We found that, on average, Fz7-YFP accumulations at the first time point of the video occupied only 70% (± 3.6% SEM) of the total cell contact length, whereas at the last time point before separation, 96% (± 2.2% SEM) was occupied (Fig. 5 D). Consistent with this, when two cells containing accumulated Fz7-YFP at their contact site moved apart, cells separated last at the site of Fz7 accumulation (Fig. 5 A; Video 1, available at http://www.jcb.org/cgi/content/full/jcb.200606017/DC1). Intriguingly, these separating cells also showed a deformation of their plasma membranes toward the remaining cell contact (Fig. 5, A and E), suggesting that the Fz7 accumulation site is resistant to separation. In contrast, cells uniformly expressing either Fz7-YFP or a membrane-tethered version of YFP (Lyn-YFP) separated more evenly along their cell contacts (Fig. 5, B and C; Videos 3 and 4). To quantify these observations, we measured the angle between contacting plasma membranes at the last time point before cell separation (illustrated in Fig. 5, E and F). Consistent with a pronounced deformation, we found a significantly bigger angle in the presence of Wnt11 (90 ± 4.4° SEM; $P < 0.05$), as compared with cells separating in the absence of Wnt11 (Fz7-YFP, 70 ± 3.73° SEM; Lyn-YFP, 65 ± 3.2° SEM; Fig. 5 F). We also observed similar separation behavior by Fz7- and Wnt11-overexpressing epiblast cells in the germ ring of shield-stage embryos (6 hpf; Video 2), where endogenous Wnt11 is expressed and active (Ulrich et al., 2003). Overall, our observations suggest that Wnt11-induced Fz7 accumulations increase the persistence of cell contacts in the immediate area.

To analyze the influence of Wnt11-induced Fz7 accumulation on cell contact persistence, we determined the rate of cell contact shrinkage during separation and the time of cell separation in the presence and absence of Fz7 accumulation (Fig. 5, G–I). Although control cells had rapid shrinkage of their cell contact length during the last phase of separation (Fz7-YFP, 1.5 ± 0.19 μm/min SEM; Lyn-YFP, 1.4 ± 0.15 μm/min SEM; Fig. 5 I and Fig. 6 I), cells containing Fz7 accumulations showed a significantly slower shrinkage rate (0.65 ± 0.06 μm/min SEM; $P < 0.05$; Fig. 5 I and Fig. 6 I). Additionally, during the timeframe of our videos (75 min), we saw consistently longer contact times and a higher percentage of cell contacts that did not separate in the presence of Fz7 accumulations (Fig. 5, G and G′). These combined differences in contact time and cell separation are given in Fig. 5 H as the ratio of cells displaying contact times longer than 30 min (including nonseparating cells) versus cells separating within the first 30 min of the video. In sum, Wnt11-induced Fz7 accumulations are associated with a local increase in cell contact persistence, most likely reflecting stronger cell adhesion at these contact sites.

Wnt11-induced Fz7 accumulations could be the cause or consequence of increased cell contact persistence. To distinguish between these two possibilities, we compared the rate of shrinkage of cell contact length to that of local Fz7 accumulations. If Fz7 accumulations are only secondary to increased cell adhesion, the length of cell contacts and Fz7 accumulations should shrink at a similar rate. In contrast, if Fz7 accumulations cause increased cell contact persistence, the rate by which Fz7 accumulations shrink should be considerably lower than the rate by which the cell contacts shrink. Consistent with Wnt11-induced Fz7 accumulations causing increased contact persistence, we found that Fz7 accumulations shrink slower than the cell contacts (Fig. 5 I).

Local increase in cell contact persistence partially depends on Flamingo, but is independent of RhoA/Rok signaling

In *D. melanogaster*, Fz and Dsh are proposed to form a signaling complex with the atypical cadherin Flamingo (Fmi) that locally directs cytoskeletal reorganization and/or adhesion (for review see Strutt, 2003). Furthermore, in zebrafish, Wnt11 and Fmi appear to cooperatively control gastrulation movements (Formstone and Mason, 2005). To determine if Fmi plays a role in the local increase of cell contact persistence resulting from Fz7 accumulation, we first analyzed zebrafish Fmi2 (also named Celsr2) localization in the animal pole assay. Fmi2 is maternally provided and zygotically expressed throughout gastrulation (unpublished data). In embryos expressing YFP-tagged Fmi2 (Fmi2-YFP), Fmi2-YFP localized at the plasma membrane and accumulated at cell contacts both with and without exogenous Wnt11 (Fig. 6, B, E, and G). Interestingly, coexpression of Fmi2-YFP with Fz7-CFP in the absence of Wnt11 resulted in the preferential accumulation of Fz7-CFP in places of increased Fmi2-YFP signal (Fig. 6, A–C). Thus, Fmi2 is able to induce

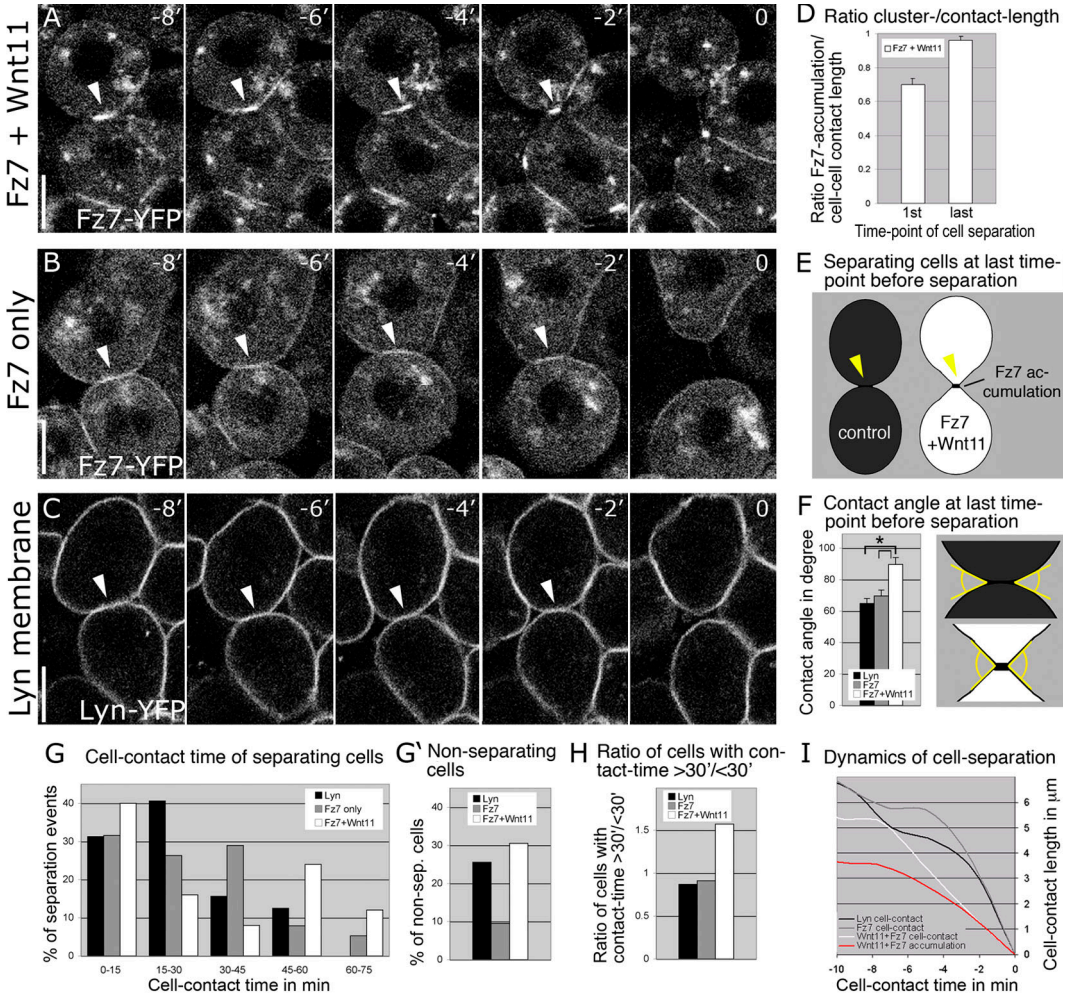

Figure 5. **Wnt11-induced accumulations of Fz7 modulate cell contact persistence.** (A–C) Time-series of separating cells in the animal pole assay expressing either a combination of *fz7-yfp* (60 pg mRNA) and *wnt11* (10 pg mRNA; A; Video 1), *fz7-yfp* alone (60 pg mRNA; B; Video 3), or *lyn-yfp* (25 pg mRNA; C; Video 4). Cells were "back-tracked" from the time point of separation (0′). Z sections shown from 3D, two-photon imaging. Time intervals are 130 (A and B) and 123 s (C); contact sites are marked by arrowheads. (D) Ratio of length of Fz7 accumulation/total cell contact length at the first video time point and last time point before separation (n = 26 out of 4 videos). Error bars represent the SEM. (E) Diagram of contacting cells containing Lyn-YFP or Fz7-YFP (control, black) versus Wnt11 + Fz7-YFP (white) at the last time point before separation. (F) Average contact angle between contacting cells at the last time point before separation. Number of cells analyzed was as follows: 34 (Fz7), 31 (Lyn), and 27 (Fz7 + Wnt11) out of 4 videos per condition. Asterisks mark statistically significant differences ($P < 0.05$). (G) Relative distribution of contact times from randomly chosen pairs of separating cells measured from start of the time-lapse until cell separation. Number of cells analyzed was as follows: 38 (Fz7), 32 (Lyn), and 25 (Fz7 + Wnt11) out of 4 videos per condition. (G′) Percentage of cells not separating within a 75-min time frame. Number of cells analyzed was as follows: 42 (Fz7), 43 (Lyn), and 36 (Fz7 + Wnt11) out of 4 videos each. (H) Ratio of cells contacting for >30 min (including nonseparating cells)/cells separating for <30 min from start of video. Calculated from data shown in G and G′. (I) Dynamic reduction of cell contact length during separation (Lyn, black; Fz7, gray; Fz7 + Wnt11, white) and reduction of Fz7 accumulation length (Fz7 + Wnt11, red). Graphs represent an average of all separation events measured per condition. Number of cells analyzed was as follows: 19 (Fz7), 26 (Lyn), and 23 (Fz7 + Wnt11) out of 4 videos per condition. t = 0 min is the first time point of separation. Bars, 10 µm. Videos 1, 3, and 4 are available at http://www.jcb.org/cgi/content/full/jcb.200606017/DC1.

accumulation of itself and Fz7 independently of Wnt11. In addition, Wnt11-CFP localized to Fmi2-YFP accumulation when coexpressed with untagged Fz7, indicating that all three components colocalize (Fig. 6, D–F). Fmi2 is therefore a likely component of Fz7/Wnt11 accumulations, possibly acting to regulate cell adhesion at cell contacts.

Using gain- and loss-of-function experiments, we investigated the role of Fmi in cell contact behavior in the animal pole assay. Cell contact persistence, as measured by the time needed for cells to separate and the percentage of nonseparating cells, was enhanced in cells expressing only Fmi2-YFP compared with cells expressing Wnt11 and Fz7 (Fig. 6, G and H–H″; Video 5, available at http://www.jcb.org/cgi/content/full/jcb.200606017/DC1). To reduce endogenous Fmi activity, we injected morpholinos (MOs) targeted against the three *fmi* genes (*fmi1a*, *fmi1b*, and *fmi2*; 4 ng/embryo each; unpublished data). In Fmi-MO–injected embryos, Wnt11/Fz7-mediated cell contact persistence was reduced (Fig. 6, H–H″; Video 6), and the shrinkage rate of cell contacts during the last phase of separation was significantly increased (0.88 µm/min ± 0.06 SEM; $P < 0.05$; Fig. 6, I and I′). Loss of Fmi function at sites of Fz7 accumulation therefore causes cells to separate faster, suggesting that Fmi contributes to Wnt11-induced Fz7 accumulation control of cell contact persistence.

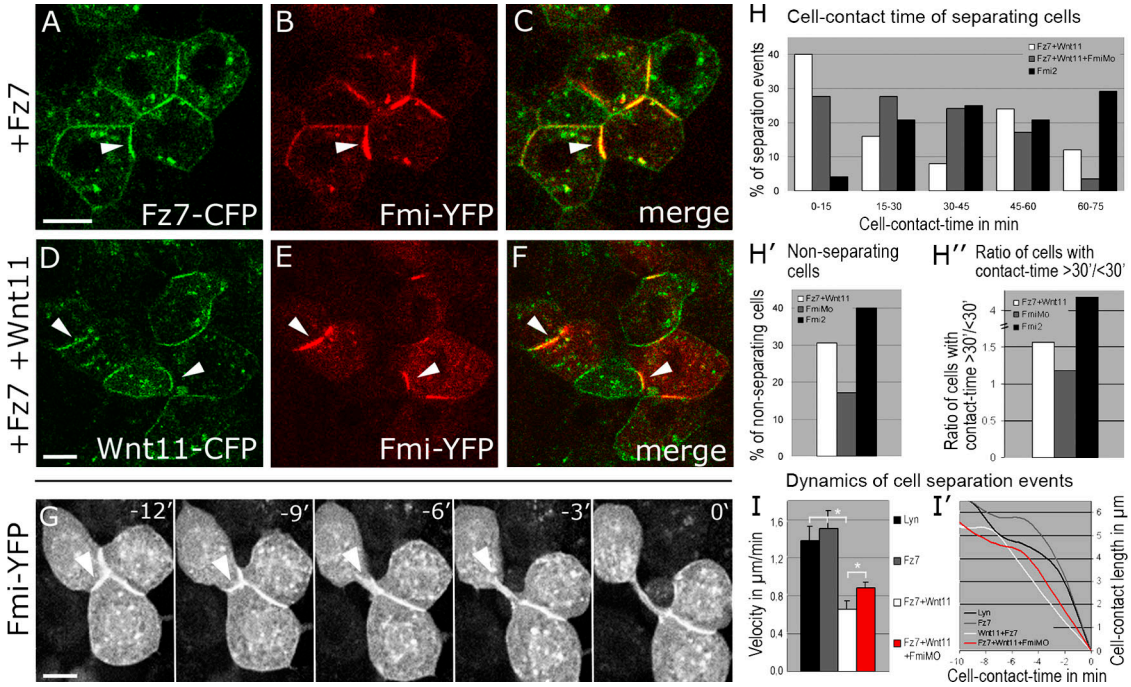

Figure 6. **Fmi2 colocalizes with Fz7 and Wnt11 at cell contacts and increases persistence.** (A–F) Animal pole assay in fixed embryos expressing a mix of *fz7-cfp* (110 pg mRNA) and *fmi2-yfp* (50 pg DNA; A–C), or a mix of *wnt11-cfp* (90 pg mRNA), *fz7* (50 pg mRNA), and *fmi2-yfp* (50 pg DNA; D–F). (A–C) Fz7-CFP (green) and Fmi2-YFP (red) colocalize in accumulations (arrowheads) at cell contacts. (D–F) Wnt11-CFP (green) and Fmi2-YFP (red) in the presence of exogenous Fz7 colocalize in accumulations (arrowheads) at cell contacts. (G) Time series of separating cells expressing Fmi2-YFP in the animal pole assay (Video 5). Fmi2-YFP accumulates (arrowheads) and remains at contacts until cell separation. Time series was obtained as described in Fig. 5, at time intervals of 171 s. (H) Relative distribution of cell contact times for separating cells expressing either *fmi2-yfp* (black), *wnt11 + fz7-yfp* (white), a combination of *wnt11 + fz7-yfp*, and MOs targeted against *fmi1a*, *fmi1b*, and *fmi2* (4 ng/MO; gray; Video 6). Cell contact times were measured as described in Fig. 5. Number of cells analyzed was as follows: 24 (Fmi2), 25 (Fz7 + Wnt11), and 29 (Fz7 + Wnt11 + FmiMO) out of 4 videos per condition. (H′) Percentage of cells not separating within 75 min. Number of cells analyzed was as follows: 40 (Fmi2), 36 (Fz7 + Wnt11), and 35 (Fz7 + Wnt11 + FmiMO) out of 4 videos per condition. (H″) Ratio of cells contacting for >30 min (including nonseparating cells)/cells separating for <30 min from start of video. Calculated from data shown in H and H′. (I and I′) Dynamic reduction of cell contact length during separation (I′), measured as described in Fig. 5. Number of cells analyzed was as follows: 19 (Fz7), 26 (Lyn), 23 (Fz7 + Wnt11), 27 (Fz7 + Wnt11 + FmiMO), and 25 (Fmi2) out of 4 videos per condition. Velocity of cell contact shrinkage (I) representing the slope of the last time point before separation to t = 0 in I′. Asterisks mark significant difference with $P < 0.05$. Error bars represent the SEM. Bars, 10 µm. Videos 5 and 6 are available at http://www.jcb.org/cgi/content/full/jcb.200606017/DC1.

Wnt11-induced Fz7 accumulations could directly affect cell contact persistence or act via downstream mediators of Wnt11 signaling, such as RhoA and Rok2 (for review see Veeman et al., 2003). To distinguish between these possibilities, we monitored the effects of Wnt11-induced Fz7 accumulations on cell contact behavior within the animal pole assay when RhoA and Rok activity is decreased. Using MOs, we "knocked down" zebrafish *rhoab* and *rhoad*, as they are expressed during gastrulation and function downstream of Wnt11 (Salas-Vidal et al., 2005; Zhu et al., 2006). To further decrease RhoA/Rok function, we incubated *rhoab/ad*-MO–injected embryos in the specific Rok inhibitor Y-27632 before image acquisition. Loss of RhoA/Rok function did not significantly interfere with the formation or effect of Fz7 accumulations on cell contact persistence (contact shrinkage rate in last phase of separation, 0.75 ± 0.14 µm/min SEM; P = 0.2; Fig. S4, available at http://www.jcb.org/cgi/content/full/jcb.200606017/DC1). This suggests that Wnt11 downstream signaling through RhoA and Rok is not directly involved in mediating enhancement of contact persistence by Wnt11-induced Fz7 accumulation.

In sum, Wnt11-induced Fz7 accumulations partially depend on Fmi to increase cell contact persistence, but are independent of Wnt11 downstream signaling through RhoA and Rok. Wnt11 may therefore directly enhance cell contact persistence via interactions with Fz7 and Fmi at the plasma membrane.

Subcellular sites of Wnt11 activity at endogenous Fz7 levels modulate contact persistence in gastrulating cells

We next wanted to determine if Wnt11 locally controls cell adhesion in gastrulating cells and whether Fz7 accumulation plays a role in such a process. We first sought to monitor endogenous Wnt11 and Fz7 activity in gastrulating cells of shield stage embryos (6 hpf) by expressing moderate amounts of Dsh-YFP in these cells. We used Dsh-YFP because (a) Fz7 recruits and colocalizes with Dsh at the plasma membrane, as seen in the animal pole assay (Fig. 4, D–F), (b) a fluorescently tagged live marker gene is needed to dynamically monitor endogenous Fz7 plasma membrane accumulation, and (c) moderate *dsh-YFP* expression (60 pg mRNA) had no obvious effect on tissue morphogenesis during gastrulation (not depicted). We analyzed Dsh-YFP localized in both epiblast cells, which endogenously express *wnt11* and *fz7* (Makita et al., 1998; Sumanas et al., 2000; El-Messaoudi and Renucci, 2001; Kudoh et al., 2001;

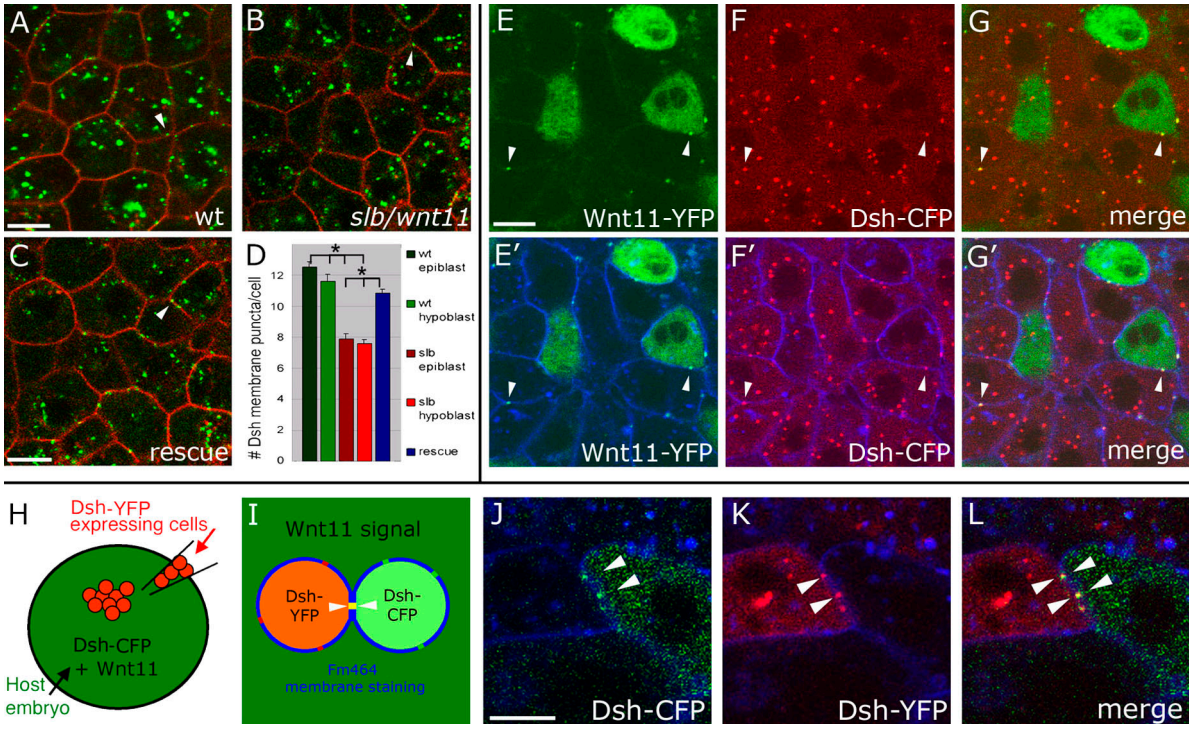

Figure 7. **Endogenous subcellular sites of Wnt11 and Fz7 activity marked by Dsh-YFP recruitment to the plasma membrane.** (A–C) Epiblast cells in germ ring of fixed gastrulating embryos (shield stage, 6 hpf) expressing *dsh-yfp* (75 pg mRNA) and *lyn-cfp* (75 pg mRNA). Dsh-YFP (green) localized in puncta (arrowheads) at the plasma membrane (red) in wild-type (A), *slb/wnt11* mutant (B), and "rescued" *slb/wnt11* mutant embryos (C; coinjected with 20 pg *wnt11* mRNA). (D) Number of Dsh-YFP puncta at the plasma membrane (for rescue condition, column represents both epiblast and hypoblast cells). Quantification performed in 3D by counting the number of Dsh-YFP puncta at the plasma membrane of a chosen cell in all z sections (step size = 1.5 μm). Number of cells analyzed was as follows (epiblast/hypoblast): 50/43 (wild type); 43/43 *(slb/wnt11* mutants); 83 (*slb/wnt11* rescue; epiblast + hypoblast) out of 6 embryos per condition. Error bars represent the SEM. (E–G′) Epiblast cells in the germ ring of living embryos (6 hpf) expressing *dsh-cfp* (100 pg mRNA), and mosaic *wnt11-yfp* mRNA (50–100 pg mRNA injection at the 16-cell–stage). Plasma membranes stained (E′–G′; blue) with FM464 by intercellular injection at 5 hpf. Wnt11-YFP (E, E′, G, and G′; green) and Dsh-CFP (F, F′, G, and G′; red) colocalize in puncta (arrowheads) at the plasma membrane (blue) of both Wnt11-producing (green cytoplasm) and receiving cells. (H–L) As diagramed (H and I), cells expressing *dsh-yfp* (60 pg mRNA; red) were transplanted into the animal pole of host embryos (4 hpf) coexpressing *dsh-cfp* (100 pg mRNA; green) and *wnt11* (50 pg mRNA). FM464 marks plasma membrane (blue). Epiblast cells imaged 3 h after transplantation within the germ ring of a living host embryo (6 hpf). (J–L) Dsh-YFP of a transplanted cell and Dsh-CFP in adjacent host cell colocalize to the same site (arrowheads). Bars, 10 μm.

Ungar and Calvey, 2002; Ulrich et al., 2003), and hypoblast cells, which endogenously express *fz7* and require Wnt11 for proper cell polarization and coherent migration (Ulrich et al., 2003, 2005).

Dsh-YFP was observed in epiblast and hypoblast cells as puncta, both in the cytoplasm and at the plasma membrane (Fig. 7 A; and not depicted), most likely reflecting dynamic Dsh assemblies (Schwarz-Romond, 2005). Localization of Dsh-YFP puncta to the plasma membrane was seen to be regulated by endogenous Wnt11 signaling, as the number of plasma membrane puncta per cell within the shield-stage germ ring (6 hpf) was reduced in *slb/wnt11* mutants (quantified in 3D; $P < 0.05$; Fig. 7, A, B, and D). Additionally, the decrease in Dsh-YFP puncta at the plasma membrane in *slb/wnt11* mutant embryos was rescued by injecting 20 pg *wnt11* mRNA ($P < 0.05$; Fig. 7, C and D). As expected, if Wnt11 is locally recruiting Dsh, we found that in embryos with ubiquitous Dsh-CFP and mosaic Wnt11-YFP expression, secreted Wnt11-YFP colocalizes with Dsh-CFP at the plasma membrane of both producing and receiving cells (Fig. 7, E–G′). This recruitment and colocalization of Wnt11 and Dsh in puncta is presumably through the function of endogenous Fz. Consistent with this, we found Dsh puncta at shield stage to localize to both contacting plasma membranes, as was shown for Fz7 in the animal pole assay (6–7 hpf; Fig. 7, H–L). Overall, Dsh-YFP puncta at the plasma membrane appear to highlight subcellular sites of endogenous Wnt11 and Fz7 activity.

It is possible that these subcellular sites of endogenous Wnt11/Fz7 activity modulate contact persistence of gastrulating cells, similar to the Wnt11-induced Fz7 accumulations in the animal pole assay. To address this possibility, we observed both puncta and separation behavior of ectodermal and mesendodermal cells within the germ ring of late shield-stage embryos (7 hpf). As Dsh puncta at the plasma membrane are only partially reduced in *slb/wnt11* mutants (Fig. 7, A–D), it is unlikely that all Dsh puncta correspond to endogenous Wnt11-induced Fz7 accumulations. Thus, to specifically address the role of Wnt11 activity under endogenous Fz7 conditions, Wnt11-YFP puncta at the plasma membrane were followed in gastrulating cells that also express the membrane marker GPI-anchored RFP (mem-RFP). We found that Wnt11 puncta localized to contact sites of separating cells and remained at the last contact point before separation (Fig. 8 A and Video 7, available at http://www.jcb.org/cgi/content/full/jcb.200606017/DC1). To compare the

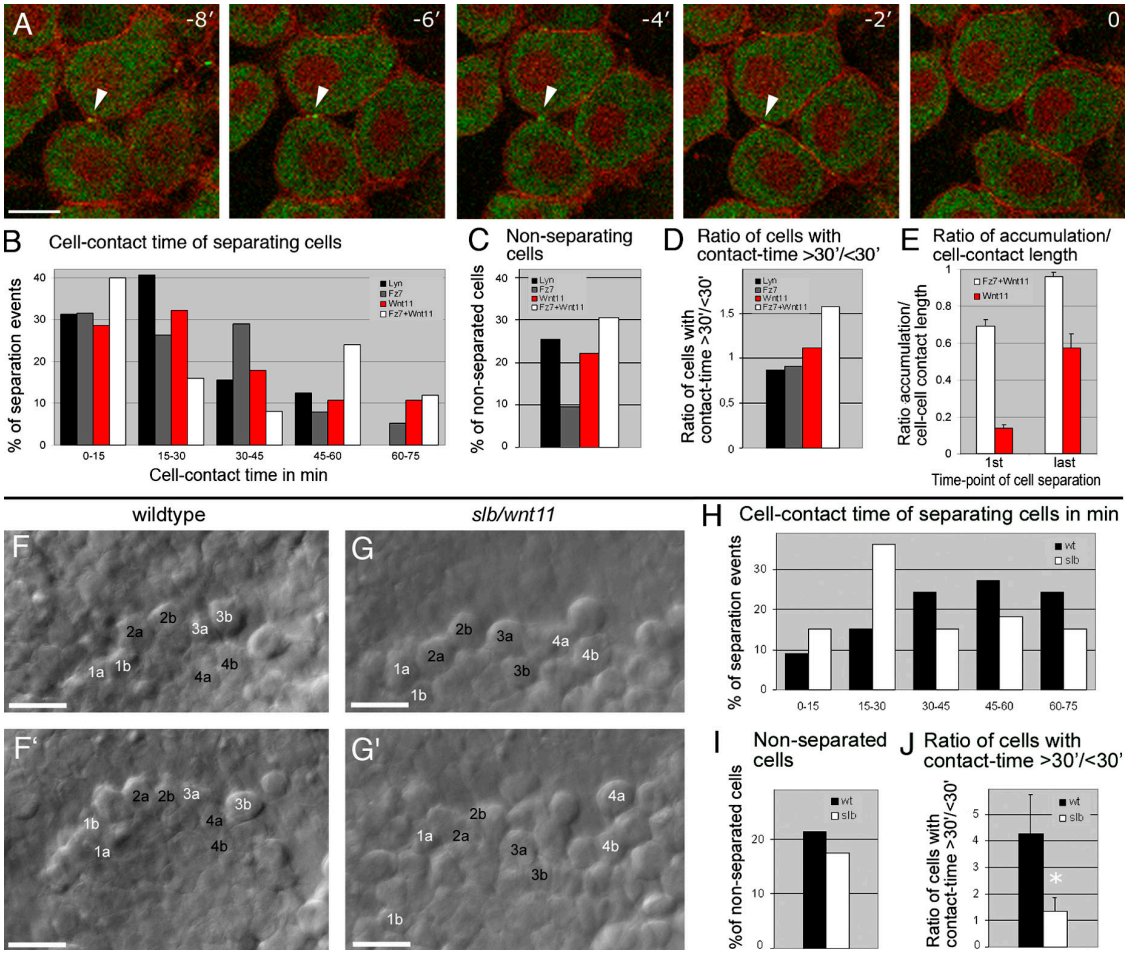

Figure 8. **Wnt11 persist at cell contacts and is required for contact persistence.** (A) Time series of separating hypoblast cells expressing a mix of 80 pg of *wnt11-yfp* and GPI-anchored *rfp* (*mem-rfp*) mRNA in shield-stage embryos (6 hpf). Wnt11-YFP (green) located in puncta at cell contacts (arrowheads) and remained until separation (Video 7). Time-series was obtained as in Fig. 5; time interval = 112 s. (B–E) Quantification of separation behavior of cells expressing Wnt11-YFP and mem-RFP (as in A, red) in animal pole assay (Video 8) compared with conditions described in Fig. 5 (G–H; Fz7-YFP + Wnt11, white; Lyn-YFP, black; Fz7-YFP, gray). (B) Relative distribution of contact times produced, as described for Fig. 5. Number of cells analyzed was as follows: 28 (Wnt11), 25 (Fz7 + Wnt11), 38 (Fz7), and 32 (Lyn) out of 4 videos per condition. (C) Percentage of cells not separating in 75 min. Number of cells analyzed was as follows: 36 (Wnt11), 36 (Fz7 + Wnt11), 42 (Fz7), and 43 (Lyn) out of 4 videos per condition. (D) Ratio of cells contacting for >30 min (including nonseparating cells)/cells separating for <30 min from start of video. Calculated from data in B and C. (E) Ratio of length of Wnt11 puncta or Fz7 accumulation/total contact length at the first video time point and the last time point before separation; number of cells analyzed was as follows: 20 (Wnt11) and 26 (Fz7 + Wnt11) out of 4 videos per condition. (F–G′) Images of 3D time-lapse videos recorded for 75-min and 30-s time-intervals in wild-type (F and F′, and Video 9) and *slb/wnt11* (G and G′, and Video 10) mutant embryos at late shield stage (7 hpf), using bright-field microscopy. "Head-on" view of the dorsal germ ring (shield) showing cells at the leading edge of the prechordal plate. Images shown are first (F and G) and last (F′ and G′) video time points. Numbers mark exemplary cells that separate (white) or remain in contact (black). (H) Relative distribution of cell contact times for separating wild-type and *slb/wnt11* mutant prechordal plate progenitors (see Videos 9 and 10). Measured in 3D and presented as described for Fig. 5. Number of cells analyzed was as follows: 33 (wild type) and 37 (*slb/wnt11*) out of 5 videos per condition. (I) Percentage of cells not separating in wild-type and *slb/wnt11* mutant embryos in 75 min. Number of cells analyzed was as follows: 42 (wild type) and 44 (*slb/wnt11*) out of 5 videos per condition. (J) Ratio of cells contacting >30 min (including nonseparating cells)/cells separating <30 min from start of video. Calculated from data in H and I. Asterisk represents the significant difference, with $P < 0.05$. Error bars represent the SEM. Bars: (A) 10 μm; (F, F′, G, and G′) 50 μm. Videos 8–10 are available at http://www.jcb.org/cgi/content/full/jcb.200606017/DC1.

effect of Wnt11 puncta on contact persistence with that of Wnt11-induced Fz7 accumulations, we also expressed Wnt11-YFP and mem-RFP in the animal pole assay. By determining the contact time of separating cells and the percentage of non-separating cells, we found that cells containing Wnt11 puncta at their contact sites exhibit increased contact persistence compared with cells expressing Lyn-YFP or Fz7-YFP (Fig. 8, B–D; and Video 8). This Wnt11 enhancement of contact persistence was considerably smaller than that of Wnt11-induced Fz7 accumulation, an expected result given the small size of Wnt11 puncta (Fig. 8, B–D). In addition, Wnt11 puncta initially occupied only 14 ± 2% SEM of the total cell contact length, but covered 57 ± 7% SEM at the last time point before separation. This indicates that Wnt11 puncta persist at the last point of cell contact, similar to Fz7 accumulations (Fig. 8 E).

In summary, these data suggest the presence of subcellular sites of endogenous Wnt11 activity at cell contacts during gastrulation. These regions, marked by Wnt11 puncta, share several features with the Wnt11-induced Fz7 accumulations described in the animal pole assay.

Contact persistence between prechordal plate progenitor cells is reduced in *slb/wnt11* mutant embryos

We previously found that Wnt11 controls directed and coherent movements of prechordal plate progenitors during gastrulation (Ulrich et al., 2005). To determine whether Wnt11 coordinates directed prechordal plate migration by regulating cell contact persistence, we compared the separation behavior of these cells in wild-type versus *slb/wnt11* mutant embryos. As expected, we saw shorter contact times in *slb/wnt11* mutants (Fig. 8, F–J; and Videos 9 and 10, available at http://www.jcb.org/cgi/content/full/jcb.200606017/DC1), and less compaction of the tissue (Fig. 8, F' and G′). These results indicate that endogenous Wnt11 function is required for cell contact persistence within the forming prechordal plate, a potential mechanism to facilitate directed and coherent movement during gastrulation.

Discussion

Central to this study is our finding that Wnt11 induces the accumulation of its receptor Fz7 and its intracellular mediator Dsh at distinct sites of cell contacts. Direct binding of Wnt11 to Fz7 may be required to trigger this accumulation, as we found that the C-terminally truncated inactive version of Wnt11 potentially lacking the binding site to Fz (Slb/Wnt11^{tx226}; Heisenberg et al., 2000) is not sufficient. This is consistent with previous data indicating that XWnt11 and XFz7 biochemically interact in *X. laevis* (Djiane et al., 2000). In addition, relocation of Dsh from the cytoplasm to sites of Fz7 accumulation presumably occurs through direct binding of Dsh to Fz7 (Wong et al., 2003).

Significantly, we demonstrate that Wnt11-induced Fz7 accumulations locally increase the persistence of cell contacts. This is based on the observations (a) that separating cells containing Fz7 accumulations at their contact sites break their cell contact last at sites of Fz7 accumulation, (b) that these cells remain in contact longer and exhibit deformation of their membranes toward the point of cell contact, and (c) that during the course of cell separation the size of Fz7 accumulations shrink slower than the total cell contact length. Therefore, we propose that Fz7 accumulations are adhesive subdomains within cell contacts.

It is unlikely that Fz7 or Wnt11 molecules directly modulate cell adhesion, nor do our data support a critical role of downstream signaling through Wnt11 effectors such as RhoA and Rok2 in this process. One possibility is that Wnt11-induced Fz7-accumulations interact with an adhesion molecule mediating these adhesive functions. Several lines of evidence point to the involvement of the atypical cadherin Fmi, a key component of PCP signaling in *D. melanogaster* (Usui et al., 1999). Previous work showed a functional interaction between Fmi and Wnt11 in controlling convergent extension movements during zebrafish gastrulation (Formstone and Mason, 2005). In addition, Fmi exhibits adhesive function in cultures of dissociated zebrafish embryonic cells, as well as in *D. melanogaster* S2 cell cultures (Usui et al., 1999; Shima et al., 2004; unpublished results). We not only found that Fmi colocalizes with Fz7 accumulations but also discovered that endogenous Fmi function is required for the cell contact persistence mediated by Fz7 accumulation. Collectively, our data strongly suggests that Fmi plays a key role in controlling cell adhesion at sites of Wnt11-induced Fz7 accumulation.

In *D. melanogaster*, localization of Fmi to proximal and distal cortices of pupal wing epithelial cells is essential for proper Fz and Dsh localization to the distal cortex (Axelrod, 2001; Shimada et al., 2001; Strutt, 2001), where a potential protein complex of Fmi, Fz, and Dsh mediates cell polarization (Strutt, 2003). Our similar finding of Fz7, Dsh, and Fmi2 colocalizing at cell contacts in zebrafish points to a shared role for subcellular distribution and function of these PCP components in *D. melanogaster* and zebrafish. Although this is an attractive hypothesis, there are also differences between PCP signaling in *D. melanogaster* and zebrafish. First, no Wnt ligand in PCP signaling has yet been identified in *D. melanogaster*. Second, although Fz7, Dsh, and Fmi2 colocalize on both contacting plasma membranes in zebrafish, only Fmi localizes to both membranes in *D. melanogaster*. Despite these differences, Fmi might serve as a common effector for PCP signaling by recruiting other PCP components to specific sites on the plasma membrane and directly regulating cell adhesion. This notion is supported by our observation in zebrafish that Fmi can promote Fz7 accumulation at cell contact sites independently of Wnt11, suggesting that Fmi, through its effect on Fz7, can determine sites of local Wnt11 activity.

How does the function of Wnt11/Fz7 in controlling cell contact persistence relate to previous findings about the morphogenetic activity of Wnt/PCP signaling in zebrafish and *D. melanogaster*? It has been proposed that Wnt/PCP signaling controls cadherin-mediated rearrangement of cells as they polarize. In *D. melanogaster*, PCP signaling mediates cadherin recycling required for the packing of wing epithelial cells into hexagonal arrays, a process accompanied by asymmetric localization of PCP components (Classen et al., 2005). Similarly in zebrafish, Wnt11-mediated E-cadherin endocytosis and recycling controls cohesion of prechordal plate progenitors required for directed and coherent cell migration (Ulrich et al., 2005). Thus, there is a basis for cadherin endocytosis/recycling serving as a common mechanism by which Wnt/PCP signaling globally regulates cell cohesion and junctional remodeling. However, Wnt/PCP components may also directly control cell contact dynamics in vertebrates. Based on this study, we propose that in zebrafish Wnt11 locally controls cell adhesion by interacting with Fz7, Dsh, and Fmi at the plasma membrane. Whether the effects of Wnt11 on Fz7 accumulation and E-cadherin endocytosis/recycling are independent activities of Wnt11 in controlling cell adhesion remains to be established.

But what is the relevance of our findings from the animal pole assay for the endogenous function of Wnt11 during zebrafish gastrulation? Our observation that Dsh recruits to sites of secreted Wnt11 puncta at the plasma membrane under endogenous levels of Fz suggests that these Dsh puncta mark sites of endogenous Wnt11/Fz activity. This is also supported by the fact that the number of Dsh puncta at the plasma membrane of germ ring cells is controlled by endogenous Wnt11. Furthermore, we found that Wnt11/Dsh puncta at cell contact sites

display properties similar to Wnt11-induced Fz7 accumulations in the animal pole assay. In particular, Wnt11/Dsh puncta (a) localize to both contacting plasma membranes, (b) occupy the last point of cell contact, and (c) enhance the persistence of cell contacts. Relating these findings to gastrulation movements, we determined that, as expected, the persistence of cell contacts between migrating prechordal plate progenitors is decreased in *slb/wnt11* mutant embryos. This is consistent with previous data showing that *slb/wnt11* mutant prechordal plate progenitors migrate less coherently and directed (Ulrich et al., 2003, 2005). In total, these findings support a critical endogenous role for Wnt11/Fz7/Dsh accumulations in promoting the local persistence of cell contacts, a mechanism by which Wnt11 controls coherent cell migration.

Interestingly, recent studies provide evidence for a connection between noncanonical Wnt signaling and focal adhesion points. In *X. laevis*, it has been shown that the transmembrane heparan sulfate proteoglycan Syndecan4 interacts with Fz7 and Dsh. Furthermore, binding of Syndecan4 to fibronectin facilitates Fz7 recruitment of Dsh to the plasma membrane and, subsequently, the activation of noncanonical Wnt signaling (Marsden and DeSimone, 2001; Munoz et al., 2006). Considering the requirement for Syndecan4 during *X. laevis* convergent extension movements (Munoz et al., 2006), as well as the colocalization of Dsh and Fz with focal adhesion components in cultured cells (Wiggan and Hamel, 2002), it is conceivable that Wnt11/Dsh puncta at the plasma membrane share similarities in composition and function with focal adhesion points. Future experiments addressing the localization and function of Syndecan4 and other focal adhesion components, in respect to Wnt11/Dsh puncta, will provide insight into the role of Wnt/PCP signaling in regulating local cell adhesion in different developmental processes.

Conclusion

We provide evidence that the Wnt/PCP signaling components Wnt11, Fz7, Dsh, and Fmi accumulate at distinct sites on the plasma membrane that act locally to enhance cell adhesion. These findings provide insight into the molecular and cellular mechanisms by which Wnt/PCP signaling regulates cell adhesion on a subcellular level during vertebrate gastrulation.

Materials and methods

Embryo maintenance

Fish maintenance and embryo collection was performed as previously described (Westerfield, 2000). For mutant analysis, we used homozygous *slb/wnt11*^{tx226} embryos (Heisenberg et al., 2000).

Constructs

Fz7a/Fz7b-YFP/CFP fusions were constructed as C-terminal fusions of zebrafish *fz7a* (NM_131139; El-Messaoudi and Renucci, 2001) and *fz7b* (NM_170763; Sumanas et al., 2000; Ungar and Calvey, 2002) cDNA fused to either *venusyfp* or *ecfp* (CLONTECH Laboratories, Inc.) as previously described for *D. melanogaster* Fz-GFP fusion (Strutt, 2001). Full-length cDNA of zebrafish *fz7b* (NM_170763; (Sumanas and Ekker, 2001; Ungar and Calvey, 2002) was amplified by PCR using a cDNA library of shield- and bud-stage embryos, followed by subcloning into pCS2+ expression vector. Wnt11-YFP/CFP fusions were constructed as C-terminal fusions of zebrafish *wnt11* cDNA (Heisenberg et al., 2000) with either *venus-yfp* (an EYFP-derivative that was provided by A. Miyawaki, RIKEN, Saitama, Japan) or *Cerulean-ecfp* (an improved eCFP-derivative; Rizzo et al., 2004). A linker sequence of nine amino acids (EFSSGSIDG) was introduced between Wnt11 and YFP/CFP. For Dsh-YFP/CFP fusion constructs, a C-terminal fusion of *X. laevis dsh* cDNA to either *venusyfp* or *ecfp* was generated by replacing the *egfp* with *yfp/cfp* of a previously described *X. laevis* dsh-egfp fusion construct (Yang-Snyder et al., 1996). For Lyn-YFP/CFP fusions (Lyn-YFP/CFP), the myristoylation membrane localization signal of Lyn tyrosine kinase was fused to the N terminus of either eCFP or venusYFP. The membrane-RFP (memRFP) construct was provided by A. Siekmann (Max-Planck-Institute for Cell Biology and Genetics, Dresden, Germany) and encodes a monomeric form of RFP, which is targeted to the plasma membrane by a GPI anchor. Zebrafish *fmi2*, the orthologue of mouse *celsr2*, was cloned from a zebrafish gastrula library, and a full-length version of Fmi2 was fused to the N terminus of venusYFP and cloned into the *pCS2+* to generate *pCS2-Fmi2-venusyfp*. Details of cloning zebrafish *fmi2* will be published elsewhere (FCB and MT, manuscript in preparation). Zebrafish FGF8 receptor fused to RFP was provided by M. Kolanczyk and M. Brand (Max-Planck-Institute for Cell Biology and Genetics, Dresden, Germany).

RNA and morpholino injection

For mRNA synthesis, pCS2+ expression vectors containing the cDNAs for different constructs were linearized by Not1 restriction digest and transcribed by Sp6 mRNA polymerase, as previously described (Montero et al., 2003). Description of mRNA amounts per experiment is stated in the figure legends. For Fmi-YFP expression, *pcs2-fmi2-venusyfp* plasmid DNA was injected in two-cell–stage embryos. To knock down RhoA function, embryos were injected with a mix of 8 ng of MO oligonucleotides directed against the zebrafish *rhoAb* (5′-TCTTGCG AATTGCTGCCATATTTGC-3′) and *rhoAd* (5′-AGCTTCTTACGGATAG CTGCCAT-3′) genes. *RhoAb* and *rhoAd* morphant embryos exhibited similar convergent extension defects, as previously reported (Zhu et al., 2006). For knocking down Fmi activity, we used MOs targeting the start codons *fmi1a*, *fmi1b*, and *fmi2*, as follows: *fmi1a* MO (5′-CATGGTGTAAAACTCCGCAAACAGG-3′), *fmi1b* MO (5′-CATCCATATCACTGGTAATTCCATG-3′), and *fmi2* MO (5′-CAAAGAGCAACAAATCCCCCTTCAT-3′)

Treatment of embryos with Rok inhibitor Y-27632

Dechorionated embryos (4 hpf) were incubated with E2-media solution containing 50 μM of the Rok-specific inhibitor Y-27632 (Tocris Bioscience). For time-lapse imaging, inhibitor-treated embryos were mounted in 1% Agarose containing the inhibitor and covered with inhibitor containing E2-media.

In situ hybridization

In situ stainings were performed as previously described (Ulrich et al., 2003; Montero et al., 2005). In situ probes were synthesized from cDNA for *hgg1*, *dlx3*, and *ntl* (Akimenko et al., 1994; Schulte-Merker et al., 1994; Thisse et al., 1994), using a DIG RNA-labeling kit (Roche).

Image acquisition and quantification

For localization studies, embryos were fixed in 4% PFA in PBS overnight at 4°C, followed by washing in PBST (PBS + 0.1% Tween20), dechorionation, and mounting in Agarose-coated dishes in PBST. Confocal images were acquired at room temperature using a TCS-SP2 confocal microscope (HCX APO L 63×/0.9 W UVI dipping objective and confocal software; both Leica). For Fig. S2, a LSM-META confocal microscope with Achroplan 40×/0.8 W dipping objective was used (Carl Zeiss MicroImaging, Inc.). For colocalization studies, CFP/YFP or GFP/RFP channels were acquired by sequential scanning. Confocal images were analyzed and quantified using Volocity 3.0 (Improvision), LSM 5 Image Browser (Carl Zeiss MicroImaging, Inc.), and ImageJ v. 1.29–1.32 (http://rsb.info.nih.gov/ij/). To analyze significance, P values were determined in Microsoft Excel (unpaired *t* test, two-tailed distribution). For time-lapse imaging, embryos were dechorionated and mounted in 1% low melting point Agarose covered with embryo media, and imaging was performed at room temperature using water-dipping lenses. Single-color, time-lapse imaging was performed by two-photon microscopy using the Radiance system and a Plan Apo 60×/1.2 WI objective (both Bio-Rad Laboratories), as previously described (Ulrich et al., 2003). For two-color, time-lapse imaging of cells expressing YFP and RFP signals, a LSM 405-/594-nm confocal microscope with C-Apochromat 63×/1.2 W correlation objective was used (Carl Zeiss MicroImaging, Inc.). YFP and RFP channels were acquired by simultaneous scanning using 488-/594-nm laser lines for excitation, and 490-/590-nm NFT filters and BP505-580-/LP610-nm filters for separation and detection of the signals. To acquire 3D time-lapse videos, defined z stacks

with a step size of 1.6–1.8 μm were recorded over a time interval of ~145 s (depending on the exact size of the z stack). 3D time-lapse videos were analyzed using Volocity 3.0 or LSM 5 Image Browser (a) by randomly choosing cell contacts from the first time frame of the videos and tracking their separation behavior in 2D (by selecting one z section/time point) until the end of the video or until cells were completely separated ("forward tracking"; Figs. 5, G and H; 6, H–H''; and 8, B–D and H–J) and (b) by selecting cell contacts that separated within the timeframe of 75 min and tracking them backward from the time point of complete separation until the first timeframe of the videos ("backward tracking"; Figs. 5 I, 6 I', and S4). Differential interference contrast time-lapse videos showing prechordal plate morphogenesis at the shield stage (6 hpf) of embryos were taken using an Axioplan2 microscope (Carl Zeiss MicroImaging, Inc.) and a 40× 0.8 WPh2 Achroplan objective, as previously described (Montero et al., 2003). To acquire 3D time-lapse videos, defined z stacks with a step size of 3–4 μm were recorded in time intervals of 30 s using Openlab imaging software (Improvison). To analyze the contact time of cells, a 4D version of Image was used to track randomly chosen cell contacts from the first time point of the videos in 3D until cells completely separated.

Online supplemental material

Table S1 lists the biological activities of Wnt11-YFP compared with Wnt11. Fig. S1 shows the expression patterns of *wnt11*, *fz7a*, and *fz7b*. Fig. S2 shows the quantification of intensity increase at Fz7 accumulations. Fig. S3 shows distribution of FGF8 receptor–RFP at Fz7 accumulations. Fig. S4 shows quantification of separation dynamics in the absence of RhoA/Rok2 function. Video1 shows separating cells expressing Fz7-YFP and Wnt11. Video2 shows separation of gastrula-stage cells expressing Fz7-YFP and Wnt11. Video 3 shows separating cells expressing Fz7-YFP. Video 4 shows separating cells expressing Lyn-YFP. Video 5 shows separating pregastrula-stage cells expressing Fmi2-YFP. Video 6 shows separating pregastrula-stage *fmi* morphant cells expressing Fz7-YFP and Wnt11. Video 7 shows separating gastrula stage cells expressing Wnt11-YFP and memRFP. Video 8 shows separating pregastrula stage cells expressing Wnt11-YFP and memRFP. Video 9 shows morphogenesis of wild-type prechordal plate progenitors. Video 10 shows morphogenesis of *slb/wnt11* mutant prechordal plate progenitors. Online supplemental material is available at http://www.jcb.org/cgi/content/full/jcb.200606017/DC1.

We are grateful to L. Rohde, M. Gonzalez-Gaitan, A. Classen, R. Moon, I. Castanon, and M. Köppen for reading earlier versions of this manuscript, and to R. Mayor for communicating data before publication. We thank H. Steinbeisser, J. Wallingford, A. Schambony, D. Wedlich, R. Moon, M. Kolanczyk, A. Siekmann and M. Brand for providing constructs. We are also grateful to J. Peychl and J. Sanderson for advice with confocal microscopy and to G. Junghanns, E. Lehmann, M. Fischer, and J. Hückmann for help with the fish care.

This work was supported by grants from the Emmy-Noether-Program of the Deutschen Forschungsgemeinschaft and the Max-Planck Society to C.P. Heisenberg and from the Medical Research Council to M. Tada.

Submitted: 5 June 2006
Accepted: 25 October 2006

References

Adler, P.N. 2002. Planar signaling and morphogenesis in *Drosophila*. *Dev. Cell*. 2:525–535.

Akimenko, M.A., M. Ekker, J. Wegner, W. Lin, and M. Westerfield. 1994. Combinatorial expression of three zebrafish genes related to distal-less: part of a homeobox gene code for the head. *J. Neurosci.* 14:3475–3486.

Axelrod, J.D. 2001. Unipolar membrane association of Dishevelled mediates Frizzled planar cell polarity signaling. *Genes Dev.* 15:1182–1187.

Classen, A.K., K.I. Anderson, E. Marois, and S. Eaton. 2005. Hexagonal packing of *Drosophila* wing epithelial cells by the planar cell polarity pathway. *Dev. Cell*. 9:805–817.

Djiane, A., J. Riou, M. Umbhauer, J. Boucaut, and D. Shi. 2000. Role of frizzled 7 in the regulation of convergent extension movements during gastrulation in *Xenopus laevis*. *Development*. 127:3091–3100.

El-Messaoudi, S., and A. Renucci. 2001. Expression pattern of the frizzled 7 gene during zebrafish embryonic development. *Mech. Dev.* 102:231–234.

Formstone, C.J., and I. Mason. 2005. Combinatorial activity of Flamingo proteins directs convergence and extension within the early zebrafish embryo via the planar cell polarity pathway. *Dev. Biol.* 282:320–335.

Heisenberg, C.P., M. Tada, G.J. Rauch, L. Saude, M.L. Concha, R. Geisler, D.L. Stemple, J.C. Smith, and S.W. Wilson. 2000. Silberblick/Wnt11 mediates convergent extension movements during zebrafish gastrulation. *Nature*. 405:76–81.

Kudoh, T., M. Tsang, N.A. Hukriede, X. Chen, M. Dedekian, C.J. Clarke, A. Kiang, S. Schultz, J.A. Epstein, R. Toyama, and I.B. Dawid. 2001. A gene expression screen in zebrafish embryogenesis. *Genome Res.* 11:1979–1987.

Makita, R., T. Mizuno, S. Koshida, A. Kuroiwa, and H. Takeda. 1998. Zebrafish Wnt11: pattern and regulation of the expression by the yolk cell and No tail activity. *Mech. Dev.* 71:165–176.

Marsden, M., and D.W. DeSimone. 2001. Regulation of cell polarity, radial intercalation and epiboly in *Xenopus*: novel roles for integrin and fibronectin. *Development*. 128:3635–3647.

Medina, A., R.K. Swain, K.M. Kuerner, and H. Steinbeisser. 2004. *Xenopus* paraxial protocadherin has signaling functions and is involved in tissue separation. *EMBO J.* 23:3249–3258.

Montero, J.A., B. Kilian, J. Chan, P.E. Bayliss, and C.P. Heisenberg. 2003. Phosphoinositide 3-kinase is required for process outgrowth and cell polarization of gastrulating mesendodermal cells. *Curr. Biol.* 13:1279–1289.

Montero, J.A., L. Carvalho, M. Wilsch-Brauninger, B. Kilian, C. Mustafa, and C.P. Heisenberg. 2005. Shield formation at the onset of zebrafish gastrulation. *Development*. 132:1187–1198.

Munoz, R., M. Moreno, C. Oliva, C. Orbenes, and J. Larrain. 2006. Syndecan-4 regulates non-canonical Wnt signalling and is essential for convergent and extension movements in *Xenopus* embryos. *Nat. Cell Biol.* 8:492–500.

Park, T.J., R.S. Gray, A. Sato, R. Habas, and J.B. Wallingford. 2005. Subcellular localization and signaling properties of dishevelled in developing vertebrate embryos. *Curr. Biol.* 15:1039–1044.

Puech, P.H., A. Taubenberger, F. Ulrich, M. Krieg, D.J. Muller, and C.P. Heisenberg. 2005. Measuring cell adhesion forces of primary gastrulating cells from zebrafish using atomic force microscopy. *J. Cell Sci.* 118:4199–4206.

Rizzo, M.A., G.H. Springer, B. Granada, and D.W. Piston. 2004. An improved cyan fluorescent protein variant useful for FRET. *Nat. Biotechnol.* 22:445–449.

Rothbacher, U., M.N. Laurent, M.A. Deardorff, P.S. Klein, K.W. Cho, and S.E. Fraser. 2000. Dishevelled phosphorylation, subcellular localization and multimerization regulate its role in early embryogenesis. *EMBO J.* 19:1010–1022.

Salas-Vidal, E., A.H. Meijer, X. Cheng, and H.P. Spaink. 2005. Genomic annotation and expression analysis of the zebrafish Rho small GTPase family during development and bacterial infection. *Genomics*. 86:25–37.

Schulte-Merker, S., F.J. van Eeden, M.E. Halpern, C.B. Kimmel, and C. Nusslein-Volhard. 1994. no tail (ntl) is the zebrafish homologue of the mouse T (Brachyury) gene. *Development*. 120:1009–1015.

Schwarz-Romond, T., C. Merrifield, B.J. Nichols, and M. Bienz. 2005. The Wnt signalling effector Dishevelled forms dynamic protein assemblies rather than stable associations with cytoplasmic vesicles. *J. Cell Sci.* 118:5269–5277.

Shima, Y., M. Kengaku, T. Hirano, M. Takeichi, and T. Uemura. 2004. Regulation of dendritic maintenance and growth by a mammalian 7-pass transmembrane cadherin. *Dev. Cell*. 7:205–216.

Shimada, Y., T. Usui, S. Yanagawa, M. Takeichi, and T. Uemura. 2001. Asymmetric colocalization of Flamingo, a seven-pass transmembrane cadherin, and Dishevelled in planar cell polarization. *Curr. Biol.* 11:859–863.

Strutt, D. 2003. Frizzled signalling and cell polarisation in *Drosophila* and vertebrates. *Development*. 130:4501–4513.

Strutt, D.I. 2001. Asymmetric localization of frizzled and the establishment of cell polarity in the *Drosophila* wing. *Mol. Cell*. 7:367–375.

Sumanas, S., and S.C. Ekker. 2001. *Xenopus* frizzled-7 morphant displays defects in dorsoventral patterning and convergent extension movements during gastrulation. *Genesis*. 30:119–122.

Sumanas, S., P. Strege, J. Heasman, and S.C. Ekker. 2000. The putative wnt receptor *Xenopus* frizzled-7 functions upstream of beta-catenin in vertebrate dorsoventral mesoderm patterning. *Development*. 127:1981–1990.

Thisse, C., B. Thisse, M.E. Halpern, and J.H. Postlethwait. 1994. Goosecoid expression in neurectoderm and mesendoderm is disrupted in zebrafish cyclops gastrulas. *Dev. Biol*. 164:420–429.

Torres, M.A., J.A. Yang-Snyder, S.M. Purcell, A.A. DeMarais, L.L. McGrew, and R.T. Moon. 1996. Activities of the *Wnt*-1 class of secreted signaling factors are antagonized by the *Wnt*-5A class and by a dominant negative cadherin in early *Xenopus* development. *J. Cell Biol.* 133:1123–1137.

Ulrich, F., M.L. Concha, P.J. Heid, E. Voss, S. Witzel, H. Roehl, M. Tada, S.W. Wilson, R.J. Adams, D.R. Soll, and C.P. Heisenberg. 2003. Slb/Wnt11 controls hypoblast cell migration and morphogenesis at the onset of zebrafish gastrulation. *Development*. 130:5375–5384.

Ulrich, F., M. Krieg, E.M. Schotz, V. Link, I. Castanon, V. Schnabel, A. Taubenberger, D. Mueller, P.H. Puech, and C.P. Heisenberg. 2005. Wnt11 functions in gastrulation by controlling cell cohesion through Rab5c and E-cadherin. *Dev. Cell*. 9:555–564.

Ungar, A.R., and C.R. Calvey. 2002. Zebrafish frizzled7b is expressed in prechordal mesoderm, brain and paraxial mesoderm. *Mech. Dev.* 118:165–169.

Unterseher, F., J.A. Hefele, K. Giehl, E.M. De Robertis, D. Wedlich, and A. Schambony. 2004. Paraxial protocadherin coordinates cell polarity during convergent extension via Rho A and JNK. *EMBO J.* 23:3259–3269.

Usui, T., Y. Shima, Y. Shimada, S. Hirano, R.W. Burgess, T.L. Schwarz, M. Takeichi, and T. Uemura. 1999. Flamingo, a seven-pass transmembrane cadherin, regulates planar cell polarity under the control of Frizzled. *Cell*. 98:585–595.

Veeman, M.T., J.D. Axelrod, and R.T. Moon. 2003. A second canon. Functions and mechanisms of beta-catenin-independent Wnt signaling. *Dev. Cell*. 5:367–377.

Warga, R.M., and C.B. Kimmel. 1990. Cell movements during epiboly and gastrulation in zebrafish. *Development*. 108:569–580.

Westerfield, M. 2000. The Zebrafish Book. A Guide For The Laboratory Use Of Zebrafish (*Danio rerio*). 4th edition. University of Oregon Press, Eugene, OR.

Wiggan, O., and P.A. Hamel. 2002. Pax3 regulates morphogenetic cell behavior in vitro coincident with activation of a PCP/non-canonical Wnt-signaling cascade. *J. Cell Sci.* 115:531–541.

Winklbauer, R., A. Medina, R.K. Swain, and H. Steinbeisser. 2001. Frizzled-7 signalling controls tissue separation during *Xenopus* gastrulation. *Nature*. 413:856–860.

Wong, H.C., A. Bourdelas, A. Krauss, H.J. Lee, Y. Shao, D. Wu, M. Mlodzik, D.L. Shi, and J. Zheng. 2003. Direct binding of the PDZ domain of Dishevelled to a conserved internal sequence in the C-terminal region of Frizzled. *Mol. Cell*. 12:1251–1260.

Yang-Snyder, J., J.R. Miller, J.D. Brown, C.J. Lai, and R.T. Moon. 1996. A frizzled homolog functions in a vertebrate Wnt signaling pathway. *Curr. Biol.* 6:1302–1306.

Zhu, S., L. Liu, V. Korzh, Z. Gong, and B.C. Low. 2006. RhoA acts downstream of Wnt5 and Wnt11 to regulate convergence and extension movements by involving effectors Rho Kinase and Diaphanous: Use of zebrafish as an in vivo model for GTPase signaling. *Cell. Signal.* 18:359–372.